Observation of charge-dependent azimuthal correlations and possible local strong parity violation in heavy-ion collisions

(STAR Collaboration) Abelev, B. I.; ...; Planinić, Mirko; ...; Poljak, Nikola; ...; Zuo, J. X.

Observation of charge-dependent azimuthal correlations and possible local strong parity violation in heavy-ion collisions

B. I. Abelev,[8] M. M. Aggarwal,[29] Z. Ahammed,[46] A. V. Alakhverdyants,[16] B. D. Anderson,[17] D. Arkhipkin,[3] G. S. Averichev,[16] J. Balewski,[21] O. Barannikova,[8] L. S. Barnby,[2] S. Baumgart,[51] D. R. Beavis,[3] R. Bellwied,[49] F. Benedosso,[26] M. J. Betancourt,[21] R. R. Betts,[8] A. Bhasin,[15] A. K. Bhati,[29] H. Bichsel,[48] J. Bielcik,[10] J. Bielcikova,[11] B. Biritz,[6] L. C. Bland,[3] I. Bnzarov,[16] B. E. Bonner,[35] J. Bouchet,[17] E. Braidot,[26] A. V. Brandin,[24] A. Bridgeman,[1] E. Bruna,[51] S. Bueltmann,[28] T. P. Burton,[2] X. Z. Cai,[39] H. Caines,[51] M. Calderón de la Barca Sánchez,[5] O. Catu,[51] D. Cebra,[5] R. Cendejas,[6] M. C. Cervantes,[41] Z. Chajecki,[27] P. Chaloupka,[11] S. Chattopadhyay,[46] H. F. Chen,[37] J. H. Chen,[17] J. Y. Chen,[50] J. Cheng,[43] M. Cherney,[9] A. Chikanian,[51] K. E. Choi,[33] W. Christie,[3] P. Chung,[11] R. F. Clarke,[41] M. J. M. Codrington,[41] R. Corliss,[21] T. M. Cormier,[49] M. R. Cosentino,[36] J. G. Cramer,[48] H. J. Crawford,[4] D. Das,[5] S. Dash,[12] M. Daugherity,[42] L. C. De Silva,[49] T. G. Dedovich,[16] M. DePhillips,[3] A. A. Derevschikov,[31] R. Derradi de Souza,[7] L. Didenko,[3] P. Djawotho,[41] V. Dzhordzhadze,[3] S. M. Dogra,[15] X. Dong,[20] J. L. Drachenberg,[41] J. E. Draper,[5] J. C. Dunlop,[3] M. R. Dutta Mazumdar,[46] L. G. Efimov,[16] E. Elhalhuli,[2] M. Elnimr,[49] J. Engelage,[4] G. Eppley,[35] B. Erazmus,[40] M. Estienne,[40] L. Eun,[30] P. Fachini,[3] R. Fatemi,[18] J. Fedorisin,[16] A. Feng,[50] P. Filip,[16] E. Finch,[51] V. Fine,[3] Y. Fisyak,[3] C. A. Gagliardi,[41] D. R. Gangadharan,[6] M. S. Ganti,[46] E. J. Garcia-Solis,[8] A. Geromitsos,[40] F. Geurts,[35] V. Ghazikhanian,[6] P. Ghosh,[46] Y. N. Gorbunov,[9] A. Gordon,[3] O. Grebenyuk,[20] D. Grosnick,[45] B. Grube,[33] S. M. Guertin,[6] K. S. F. F. Guimaraes,[36] A. Gupta,[15] N. Gupta,[15] W. Guryn,[3] B. Haag,[5] T. J. Hallman,[3] A. Hamed,[41] J. W. Harris,[51] M. Heinz,[51] S. Heppelmann,[30] A. Hirsch,[32] E. Hjort,[20] A. M. Hoffman,[21] G. W. Hoffmann,[42] D. J. Hofman,[8] R. S. Hollis,[8] H. Z. Huang,[6] T. J. Humanic,[27] L. Huo,[41] G. Igo,[6] A. Iordanova,[8] P. Jacobs,[20] W. W. Jacobs,[14] P. Jakl,[11] C. Jena,[12] F. Jin,[39] C. L. Jones,[21] P. G. Jones,[2] J. Joseph,[17] E. G. Judd,[4] S. Kabana,[40] K. Kajimoto,[42] K. Kang,[43] J. Kapitan,[11] K. Kauder,[8] D. Keane,[17] A. Kechechyan,[16] D. Kettler,[48] V. Yu. Khodyrev,[31] D. P. Kikola,[20] J. Kiryluk,[20] A. Kisiel,[47] S. R. Klein,[20] A. G. Knospe,[51] A. Kocoloski,[21] D. D. Koetke,[45] J. Konzer,[32] M. Kopytine,[17] I. Koralt,[28] W. Korsch,[18] L. Kotchenda,[24] V. Kouchpil,[11] P. Kravtsov,[24] V. I. Kravtsov,[31] K. Krueger,[1] M. Krus,[10] L. Kumar,[29] P. Kurnadi,[6] M. A. C. Lamont,[3] J. M. Landgraf,[3] S. LaPointe,[49] J. Lauret,[3] A. Lebedev,[3] R. Lednicky,[16] C.-H. Lee,[33] J. H. Lee,[3] W. Leight,[21] M. J. LeVine,[3] C. Li,[37] N. Li,[50] Y. Li,[43] G. Lin,[51] S. J. Lindenbaum,[25] M. A. Lisa,[27] F. Liu,[50] H. Liu,[5] J. Liu,[35] L. Liu,[50] T. Ljubicic,[3] W. J. Llope,[35] R. S. Longacre,[3] W. A. Love,[3] Y. Lu,[37] T. Ludlam,[3] G. L. Ma,[39] Y. G. Ma,[39] D. P. Mahapatra,[12] R. Majka,[51] O. I. Mall,[5] L. K. Mangotra,[15] R. Manweiler,[45] S. Margetis,[17] C. Markert,[42] H. Masui,[20] H. S. Matis,[20] Yu. A. Matulenko,[31] D. McDonald,[35] T. S. McShane,[9] A. Meschanin,[31] R. Milner,[21] N. G. Minaev,[31] S. Mioduszewski,[41] A. Mischke,[26] B. Mohanty,[46] D. A. Morozov,[31] M. G. Munhoz,[36] B. K. Nandi,[13] C. Nattrass,[51] T. K. Nayak,[46] J. M. Nelson,[2] P. K. Netrakanti,[32] M. J. Ng,[4] L. V. Nogach,[31] S. B. Nurushev,[31] G. Odyniec,[20] A. Ogawa,[3] H. Okada,[3] V. Okorokov,[24] D. Olson,[20] M. Pachr,[10] B. S. Page,[14] S. K. Pal,[46] Y. Pandit,[17] Y. Panebratsev,[16] T. Pawlak,[47] T. Peitzmann,[26] V. Perevoztchikov,[3] C. Perkins,[4] W. Peryt,[47] S. C. Phatak,[12] P. Pile,[3] M. Planinic,[52] M. A. Ploskon,[20] J. Pluta,[47] D. Plyku,[28] N. Poljak,[52] A. M. Poskanzer,[20] B. V. K. S. Potukuchi,[15] D. Prindle,[48] C. Pruneau,[49] N. K. Pruthi,[29] P. R. Pujahari,[13] J. Putschke,[51] R. Raniwala,[34] S. Raniwala,[34] R. L. Ray,[42] R. Redwine,[21] R. Reed,[5] A. Ridiger,[24] H. G. Ritter,[20] J. B. Roberts,[35] O. V. Rogachevskiy,[16] J. L. Romero,[5] A. Rose,[20] C. Roy,[40] L. Ruan,[3] M. J. Russcher,[26] R. Sahoo,[40] S. Sakai,[6] I. Sakrejda,[20] T. Sakuma,[21] S. Salur,[20] J. Sandweiss,[51] J. Schambach,[42] R. P. Scharenberg,[32] N. Schmitz,[22] J. Seele,[21] J. Seger,[9] I. Selyuzhenkov,[14] Y. Semertzidis,[3] P. Seyboth,[22] E. Shahaliev,[16] M. Shao,[37] M. Sharma,[49] S. S. Shi,[50] X.-H. Shi,[39] E. P. Sichtermann,[20] F. Simon,[22] R. N. Singaraju,[46] M. J. Skoby,[32] N. Smirnov,[51] P. Sorensen,[3] J. Sowinski,[14] H. M. Spinka,[1] B. Srivastava,[32] T. D. S. Stanislaus,[45] D. Staszak,[6] M. Strikhanov,[24] B. Stringfellow,[32] A. A. P. Suaide,[36] M. C. Suarez,[8] N. L. Subba,[17] M. Sumbera,[11] X. M. Sun,[20] Y. Sun,[37] Z. Sun,[19] B. Surrow,[21] T. J. M. Symons,[20] A. Szanto de Toledo,[36] J. Takahashi,[7] A. H. Tang,[3] Z. Tang,[37] L. H. Tarini,[49] T. Tarnowsky,[23] D. Thein,[42] J. H. Thomas,[20] J. Tian,[39] A. R. Timmins,[49] S. Timoshenko,[24] D. Tlusty,[11] M. Tokarev,[16] V. N. Tram,[20] S. Trentalange,[6] R. E. Tribble,[41] O. D. Tsai,[6] J. Ulery,[32] T. Ullrich,[3] D. G. Underwood,[1] G. Van Buren,[3] G. van Nieuwenhuizen,[21] J. A. Vanfossen Jr.,[17] R. Varma,[13] G. M. S. Vasconcelos,[7] A. N. Vasiliev,[31] F. Videbaek,[3] Y. P. Viyogi,[46] S. Vokal,[16] S. A. Voloshin,[49] M. Wada,[42] M. Walker,[21] F. Wang,[32] G. Wang,[6] H. Wang,[23] J. S. Wang,[19] Q. Wang,[32] X. Wang,[43] X. L. Wang,[37] Y. Wang,[43] G. Webb,[18] J. C. Webb,[45] G. D. Westfall,[23] C. Whitten Jr.,[6] H. Wieman,[20] S. W. Wissink,[14] R. Witt,[44] Y. Wu,[50] W. Xie,[32] N. Xu,[20] Q. H. Xu,[38] Y. Xu,[37] Z. Xu,[3] Y. Yang,[19] P. Yepes,[35] K. Yip,[3] I.-K. Yoo,[33] Q. Yue,[43] M. Zawisza,[47] H. Zbroszczyk,[47] W. Zhan,[19] S. Zhang,[39] W. M. Zhang,[17] X. P. Zhang,[20] Y. Zhang,[20] Z. P. Zhang,[37] Y. Zhao,[37] C. Zhong,[39] J. Zhou,[35] X. Zhu,[43] R. Zoulkarneev,[16] Y. Zoulkarneeva,[16] and J. X. Zuo[39]

(STAR Collaboration)

[1]*Argonne National Laboratory, Argonne, Illinois 60439, USA*

[2]*University of Birmingham, Birmingham, United Kingdom*

[3]*Brookhaven National Laboratory, Upton, New York 11973, USA*

[4]*University of California, Berkeley, California 94720, USA*

[5]*University of California, Davis, California 95616, USA*

[6]*University of California, Los Angeles, California 90095, USA*

[7]*Universidade Estadual de Campinas, Sao Paulo, Brazil*

[8]*University of Illinois at Chicago, Chicago, Illinois 60607, USA*

[9]*Creighton University, Omaha, Nebraska 68178, USA*
[10]*Czech Technical University in Prague, FNSPE, Prague CZ-115 19, Czech Republic*
[11]*Nuclear Physics Institute AS CR, Řež/Prague CZ-250 68, Czech Republic*
[12]*Institute of Physics, Bhubaneswar 751005, India*
[13]*Indian Institute of Technology, Mumbai, India*
[14]*Indiana University, Bloomington, Indiana 47408, USA*
[15]*University of Jammu, Jammu 180001, India*
[16]*Joint Institute for Nuclear Research, Dubna, RU-141 980, Russia*
[17]*Kent State University, Kent, Ohio 44242, USA*
[18]*University of Kentucky, Lexington, Kentucky, 40506-0055, USA*
[19]*Institute of Modern Physics, Lanzhou, China*
[20]*Lawrence Berkeley National Laboratory, Berkeley, California 94720, USA*
[21]*Massachusetts Institute of Technology, Cambridge, Massachusetts 02139-4307, USA*
[22]*Max-Planck-Institut für Physik, Munich, Germany*
[23]*Michigan State University, East Lansing, Michigan 48824, USA*
[24]*Moscow Engineering Physics Institute, Moscow, Russia*
[25]*City College of New York, New York, New York 10031, USA*
[26]*NIKHEF and Utrecht University, Amsterdam, The Netherlands*
[27]*Ohio State University, Columbus, Ohio 43210, USA*
[28]*Old Dominion University, Norfolk, Virginia 23529, USA*
[29]*Panjab University, Chandigarh 160014, India*
[30]*Pennsylvania State University, University Park, Pennsylvania 16802, USA*
[31]*Institute of High Energy Physics, Protvino, Russia*
[32]*Purdue University, West Lafayette, Indiana 47907, USA*
[33]*Pusan National University, Pusan, Republic of Korea*
[34]*University of Rajasthan, Jaipur 302004, India*
[35]*Rice University, Houston, Texas 77251, USA*
[36]*Universidade de Sao Paulo, Sao Paulo, Brazil*
[37]*University of Science & Technology of China, Hefei 230026, China*
[38]*Shandong University, Jinan, Shandong 250100, China*
[39]*Shanghai Institute of Applied Physics, Shanghai 201800, China*
[40]*SUBATECH, Nantes, France*
[41]*Texas A&M University, College Station, Texas 77843, USA*
[42]*University of Texas, Austin, Texas 78712, USA*
[43]*Tsinghua University, Beijing 100084, China*
[44]*United States Naval Academy, Annapolis, Maryland 21402, USA*
[45]*Valparaiso University, Valparaiso, Indiana 46383, USA*
[46]*Variable Energy Cyclotron Centre, Kolkata 700064, India*
[47]*Warsaw University of Technology, Warsaw, Poland*
[48]*University of Washington, Seattle, Washington 98195, USA*
[49]*Wayne State University, Detroit, Michigan 48201, USA*
[50]*Institute of Particle Physics, CCNU (HZNU), Wuhan 430079, China*
[51]*Yale University, New Haven, Connecticut 06520, USA*
[52]*University of Zagreb, Zagreb HR-10002, Croatia*

(Received 10 September 2009; published 28 May 2010)

Parity ($\mathcal{P}$)-odd domains, corresponding to nontrivial topological solutions of the QCD vacuum, might be created during relativistic heavy-ion collisions. These domains are predicted to lead to charge separation of quarks along the orbital momentum of the system created in noncentral collisions. To study this effect, we investigate a three-particle mixed-harmonics azimuthal correlator which is a $\mathcal{P}$-even observable, but directly sensitive to the charge-separation effect. We report measurements of this observable using the STAR detector in Au + Au and Cu + Cu collisions at $\sqrt{s_{NN}} = 200$ and 62 GeV. The results are presented as a function of collision centrality, particle separation in rapidity, and particle transverse momentum. A signal consistent with several of the theoretical expectations is detected in all four data sets. We compare our results to the predictions of existing event generators and discuss in detail possible contributions from other effects that are not related to $\mathcal{P}$ violation.

DOI: 10.1103/PhysRevC.81.054908 PACS number(s): 11.30.Er, 11.30.Qc, 25.75.Ld, 25.75.Nq

I. INTRODUCTION

Quantum chromodynamics (QCD) is widely accepted as the theory of the strong interaction. The perturbative regime, applying to processes with large momentum transfer, is theoretically calculable and has been extensively tested [1]. However, the regime in which quarks and gluons interact with modest momenta and with an effective coupling constant that is too large for perturbation theory to apply cannot be reliably calculated by analytic methods. Lattice gauge theory is one first-principle approach that can be used. It predicts the existence of a new state of strongly interacting matter at high energy density. This state has now been observed in high-energy heavy-ion collisions at the Relativistic Heavy Ion Collider (RHIC) at Brookhaven National Laboratory [2].

Many interesting features of this new state of matter produced in these collisions have been observed. In this article we focus on a new phenomenon that we refer to as local strong parity ($\mathcal{P}$) violation. It is well known that the strong interaction conserves parity—meaning that strong interactions do not lead to reactions that produce a finite expectation value for any $\mathcal{P}$-odd (changing sign under parity transformation) observable. The best evidence for this comes from experiments that set limits on the electric dipole moment of the neutron [3,4]. These experiments show that the parameter θ whose nonzero value would describe $\mathcal{P}$ violation in QCD must have magnitude less than 10^{-10}. This limit effectively makes direct global $\mathcal{P}$ violation unobservable in heavy-ion reactions. Our measurement of a similar $\mathcal{P}$-odd observable is consistent with zero at the level of the experimental precision of 10^{-4} (see Sec. VI).

The concept of local $\mathcal{P}$ violation at high temperatures or in high-energy heavy-ion collisions was discussed by Lee and Wick [5,6] and Morley and Schmidt [7] and elaborated by Kharzeev *et al.* [8]. In a dense highly excited state, gluon fields can produce configurations, local in space and time, that cause $\mathcal{P}$, time reversal $\mathcal{T}$, and, via the CPT theorem, $\mathcal{CP}$-violating effects. These field configurations form in different ways in different events, and averaged over many events they would not yield a finite expectation value for a $\mathcal{P}$-odd observable. Each space-time region, occupied by such a configuration, is spontaneously produced with a random sign of $\mathcal{P}$ violation, which in the theory is determined by the gluonic field topological charge.[1] Field configurations with nonzero topological charge have a finite expectation value for $\langle \vec{E}_{\rm chromo} \cdot \vec{B}_{\rm chromo} \rangle$, where $\vec{E}_{\rm chromo}$ and $\vec{B}_{\rm chromo}$ are the chromoelectric and chromomagnetic fields, and the average is taken over the region occupied by the configuration. Because the space-time symmetries of chromodynamic fields are the same as those of electromagnetic fields, with electric field being a vector and magnetic field being a pseudovector, this region is not invariant under $\mathcal{P}$ (and $\mathcal{T}$) transformations. Quark interactions with such topological gluonic configurations change the quark chirality, leading to asymmetry in the number of left- and right-handed quarks, $N_L - N_R = 2n_f Q$, where n_f is the number of light quark flavors and Q is the topological charge of the gluonic configuration. Thus, the gluonic field configurations with nonzero topological charge induce the local $\mathcal{P}$-violating effects. Different aspects of an experimental detection of this phenomenon were discussed in Refs. [8,11,12].

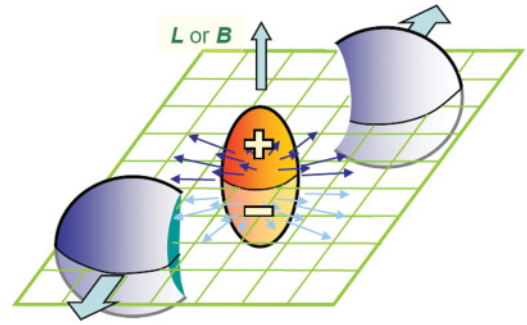

FIG. 1. (Color online) Schematic view of the charge separation along the system orbital momentum. The orientation of the charge separation fluctuates in accord with the sign of the topological charge. The direction of the orbital momentum **L**, and that of the magnetic field **B**, is indicated by an arrow.

In noncentral collisions such a domain can manifest itself via preferential same-charge particle emission along the system angular momentum [13,14] (see Fig. 1). Opposite-charge quarks would tend to be emitted in opposite directions relative to the system angular momentum. This asymmetry in the emission of quarks would be reflected in, for example, an analogous asymmetry between positive- and negative-pion emission directions. This phenomenon is driven by the large (electro-) magnetic field produced in noncentral heavy-ion collisions [13,15,16]. Peak magnetic field strengths can reach levels of the order of 10^{15} T. The combined effect of this magnetic field (which tends to align the magnetic moments of the quarks with the field) and the difference in the number of quarks with positive and negative chiralities (which is induced by their presence in a "$\mathcal{P}$-violating bubble") gives rise to the "chiral magnetic effect".

The same phenomenon can also be described in terms of induction of electric field by the (quasi) static magnetic field, which occurs in the presence of these topologically nontrivial vacuum solutions [16]. The induced electric field is parallel to the magnetic field and leads to the charge separation in that direction. Thus, the charge separation can be viewed as a nonzero electric dipole moment of the system (see Fig. 1).

Depending on the sign of the domain's topological charge, positively charged particles will be preferentially emitted either along or in the direction opposite to the system orbital angular momentum, with negative particles flowing oppositely to the positive particles. The magnetic field and the angular momentum are normal to the plane containing the trajectories of the two colliding ions. This plane, called the reaction plane, can be found experimentally in each collision by observation of the azimuthal distribution of produced particles in that event.

[1]The topological charge distinguishes gluonic-field configurations that cannot be continuously transformed one into another. In general, it is not expected to be "neutralized" and in a given event the net topological charge can take nonzero values. For a review of topological effects in QCD, see Refs. [9,10].

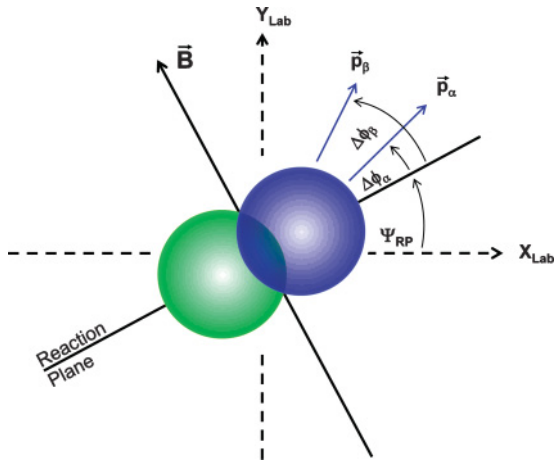

FIG. 2. (Color online) Schematic view of the transverse plane indicating the orientation of the reaction plane and particle azimuths relative to that plane. The colliding nuclei are traveling into and out of the figure.

When two heavy ions collide with a finite impact parameter, the probability for particles to be emitted in a given azimuthal direction is often described with a Fourier decomposition [17],

$$\frac{dN_\alpha}{d\phi} \propto 1 + 2v_{1,\alpha}\cos(\Delta\phi) + 2\,v_{2,\alpha}\cos(2\Delta\phi) + \cdots, \qquad (1)$$

where $\Delta\phi = (\phi - \Psi_{\rm RP})$ is the particle azimuthal direction relative to the reaction plane, as shown in Fig. 2. v_1 and v_2 are coefficients accounting for the so-called directed and elliptic flow, respectively, and α indicates the particle type. They depend on the impact parameter of the colliding nuclei, the particle type ($\pi, K, p, \ldots$), transverse momentum (p_t), and pseudorapidity (η) of the produced particles. For collisions of identical nuclei, symmetry requires v_1 to be an odd function of rapidity and v_2 to be an even function of rapidity. Measurements (for a review and references, see Ref. [18]) have found that, at RHIC, v_1 is quite small at midrapidity; typically, $|v_1| < 0.005$ for $-1 < \eta < +1$. In contrast, v_2 is found to be sizable and positive. In Au + Au collisions at $\sqrt{s_{NN}} =$ 200 GeV, for unidentified charged hadrons, v_2 reaches 0.25 for $p_t \sim 3$ GeV/c, and 0.06 when integrated over all p_t.

Phenomenologically, the charge separation owing to a domain with a given sign of the topological charge can be described by adding $\mathcal{P}$-odd sine terms to the Fourier decomposition Eq. (1) [19]:

$$\frac{dN_\alpha}{d\phi} \propto 1 + 2v_{1,\alpha}\cos(\Delta\phi) + 2\,v_{2,\alpha}\cos(2\Delta\phi) + \cdots + 2a_{1,\alpha}\sin(\Delta\phi) + 2\,a_{2,\alpha}\sin(2\Delta\phi) + \cdots, \qquad (2)$$

where the a parameters describe the $\mathcal{P}$-violating effect. Equation (2) describes the azimuthal distribution of particles of a given transverse momentum and rapidity and, like the flow coefficients, a coefficients depend on transverse momentum and rapidity of the particles. In addition, they depend also on the rapidity (position) of the domain. One expects that only particles close in rapidity to the domain position are affected. According to the theory, the signs of a coefficients vary following the fluctuations in the domain's topological charge. If the particle distributions are averaged over many events, then these coefficients will vanish because the distributions are averaged over several domains with different signs of the topological charge. However, the effect of these domains on charged-particle correlations will not vanish in this average, as discussed later in this article. In this analysis we consider only the first harmonic coefficient a_1, which is expected to account for most of the effect, although higher harmonics determine the exact shape of the distribution. For brevity we will omit the harmonic number and write $a_\alpha = a_{1,\alpha}$. The index α takes only two values, + and −, for positively and negatively charged particles, respectively.

The effects of local $\mathcal{P}$ violation cannot be significantly observed in a single event because of the statistical fluctuations in the large number of particles, which are not affected by the $\mathcal{P}$-violating fields. The average of a_α over many events, $\langle a_\alpha\rangle$, must be zero. The observation of the effect is possible only via correlations, for example, measuring $\langle a_\alpha a_\beta\rangle$ with the average taken over all events in a given event sample. The correlator $\langle a_\alpha a_\beta\rangle$ is, however, a $\mathcal{P}$-even quantity, and an experimental measurement of this quantity may contain contributions from effects unrelated to $\mathcal{P}$ violation. The correlator $\langle a_\alpha a_\beta\rangle$ can be in principle evaluated via measuring $\langle \sin\Delta\phi_\alpha \sin\Delta\phi_\beta\rangle$ with the average in the last expression taken over all pairs of particles of a given type from a kinematic region under study and then over all events. The problem is that this form of correlator contains also a large contribution from correlations not related to the reaction plane orientation (such correlations are not accounted for by Eq. (2), which is a single-particle distribution). For example, a pair of particles originating from a single jet will typically be emitted with a small azimuthal separation. These particle pairs will make a positive contribution to $\langle \sin\Delta\phi_\alpha \sin\Delta\phi_\beta\rangle$, even if the parent jets are emitted isotropically relative to the reaction plane. Therefore, we separate

$$\langle \sin\Delta\phi_\alpha \sin\Delta\phi_\beta\rangle = \langle a_\alpha a_\beta\rangle + B_{\rm out}, \qquad (3)$$

where $\langle a_\alpha a_\beta\rangle$ is caused by $\mathcal{P}$ violation and $B_{\rm out}$ (defined by this expression) includes all other correlations projected onto the direction perpendicular to the reaction plane ("out of plane"). The effects contributing to $B_{\rm out}$ may be large and are difficult to estimate reliably. For this reason, a different correlator was proposed [19]:

$$\langle\cos(\phi_\alpha + \phi_\beta - 2\Psi_{\rm RP})\rangle \qquad (4)$$

$$= \langle\cos\Delta\phi_\alpha \cos\Delta\phi_\beta\rangle - \langle\sin\Delta\phi_\alpha \sin\Delta\phi_\beta\rangle$$

$$= [\langle v_{1,\alpha}v_{1,\beta}\rangle + B_{in}] - [\langle a_\alpha a_\beta\rangle + B_{\rm out}], \qquad (5)$$

where, similarly to Eq. (3), $B_{\rm in}$ is defined via

$$\langle\cos\Delta\phi_\alpha \cos\Delta\phi_\beta\rangle = \langle v_{1,\alpha}v_{1,\beta}\rangle + B_{\rm in}. \qquad (6)$$

The correlator Eq. (4) represents the difference between correlations of the projections of the particle transverse momentum unit vectors onto an axis in the reaction plane and the correlations of the projections onto an axis that is out of plane or perpendicular to the reaction plane. The key advantage of using Eq. (5) is that it removes all the correlations among particles α and β that are not related to the reaction-plane orientation [20,21].

The contribution given by the term $\langle v_{1,\alpha} v_{1,\beta} \rangle$ can be neglected because directed flow averages to zero in a rapidity region symmetric with respect to midrapidity, as used in this analysis, and the contribution owing to directed flow fluctuations is very small (see Sec. VII for a quantitative estimate). Equation (5) then implies that by using $\langle \cos(\phi_\alpha + \phi_\beta - 2\Psi_{\rm RP}) \rangle$ instead of $\langle \sin \Delta\phi_\alpha \sin \Delta\phi_\beta \rangle$, the background to our measurement of $\langle a_\alpha a_\beta \rangle$ is now not $B_{\rm out}$, but $[B_{\rm out} - B_{\rm in}]$, where $B_{\rm in}$ is the contribution of the in-plane correlations which are analogous to $B_{\rm out}$. Only the parts of such correlations that depend on azimuthal orientation with respect to the reaction plane remain as backgrounds. Studies of the various physics contributions to $[B_{\rm out} - B_{\rm in}]$ are discussed in detail in Sec. VII.

Based on the current theoretical understanding of the chiral magnetic effect, one might expect the following features of the correlator $\langle a_\alpha a_\beta \rangle$:

(i) *Magnitude*. The first estimates [13] predicted a signal of the order of $|a| \sim Q/N_{\pi^+}$, where $Q = 0, \pm 1, \pm 2, \ldots$ is the net topological charge and N_{π^+} is the positive pion multiplicity in one unit of rapidity (the expected rapidity scale for correlations due to topological domains; see later in this article). More accurate estimates [15], including the strength of the magnetic field and topological domains production rates, were found to be close to the same number. It corresponds to values of $|a|$ of the order of 10^{-2} for midcentral collisions and to 10^{-4} for the correlator $\langle a_\alpha a_\beta \rangle$.

(ii) *Charge combinations*. If the particles, after leaving the domain, experience no medium effects (reinteraction with other particles in the system), one would expect $a_+ = -a_-$. Thus, in the absence of medium effects, one expects $\langle a_+ a_+ \rangle = \langle a_- a_- \rangle = -\langle a_+ a_- \rangle > 0$. If the process occurs in a dense medium, one needs to account for correlation modifications owing to particle interaction with the medium [15]. The effect of these modifications is similar to the modification of the jetlike two-particle correlations which experience strong suppression of the back-to-back correlations: $\langle a_+ a_+ \rangle = \langle a_- a_- \rangle \gg -\langle a_+ a_- \rangle$. The effect of strong radial flow can further modify this relation such that the opposite-charge correlations can even become positive.

(iii) *Centrality dependence.* Under the assumption that the average size of the $\mathcal{P}$-violating domain does not change with centrality, the correlator should follow a $1/N$ dependence (typical for any kind of correlations owing to clusters; N is the multiplicity) multiplied by a factor accounting for the variation of the magnetic field. The latter is difficult to predict reliably at present, other than that it should be zero in perfectly central collisions. Thus, at large centralities the effect should decrease with centrality somewhat faster than $1/N$.

(iv) *Rapidity dependence.* The correlated particles are produced in a domain of the order of 1 fm, and it is expected that the correlations should have a width in $\Delta\eta = |\eta_\alpha - \eta_\beta|$ of the order unity, as is typical for hadronic production from clusters [22].

(v) *Transverse momentum dependence.* Local $\mathcal{P}$ violation is nonperturbative in nature and the main contribution to the signal should "come from particles which have transverse momentum smaller than 1 GeV/c" [15]. The actual limits might be affected by the radial flow.

(vi) *Beam species dependence.* The effect should be proportional to the square Z^2 of the nuclear charge, but the atomic number A dependence is not well understood. One qualitative prediction is that the suppression of the back-to-back correlations should be smaller in collisions of lighter nuclei.

(vii) *Collision energy dependence.* The effect might be stronger at lower energies, as the time integral of the magnetic field is larger. At the same time, the charge separation effect is expected to depend strongly on deconfinement and chiral symmetry restoration [15], and the signal might be greatly suppressed or completely absent at an energy below that at which a quark-gluon plasma can be formed.

The main systematic uncertainty in application of the correlator Eq. (4) to measurements of anisotropies in particle production with respect to the reaction plane is due to processes when particles α and β are products of a cluster (e.g., resonance, jet) decay and the cluster itself exhibits elliptic flow [21,23]. Detailed discussion of this and other effects which could mimic the effect of local strong $\mathcal{P}$ violation in experimental measurements is presented in Sec. VII.

In this article, we report our measurements of correlators shown in Eqs. (4) and (5) and present systematic studies of the background effects that affect the measurements. Section II discusses the experimental setup, while Sec. III discusses the observables and the methods for estimating the reaction plane angle and corrections for finite reaction-plane resolution. Sections IV and V present the data and a discussion of systematic effects that can affect the measurements. Our main results, and how they systematically change with system size, centrality, particle transverse momentum, and separation in rapidity, are presented in Sec. VI. Physics backgrounds that can mimic the $\mathcal{P}$-violating effect are discussed in Sec. VII.

II. EXPERIMENTAL SETUP AND DATA TAKING

The data were collected with the STAR detector at Brookhaven National Laboratory during the 2004 and 2005 runs. Collisions of Au + Au and Cu + Cu beams were recorded at $\sqrt{s_{NN}} = 200$ and 62 GeV incident energies, for a total of four beam-energy combinations. Charged-particle tracks were reconstructed in a cylindrical time projection chamber (TPC) [24,25]. The TPC is a 4.2-m-long barrel with a 2-m radius which was operated in a solenoidal magnetic field of 0.5 T. The TPC detects charged tracks with pseudorapidity $|\eta| < 1.2$ and $p_t > 100$ MeV/c with an absolute efficiency that ranges from 80% to 90%. The TPC is nearly azimuthally symmetric and records tracks at all azimuthal angles; however, sector boundaries and other regular detector features are responsible for an approximately 10% loss of particles due to the finite acceptance of the detector. Track merging and other tracking artifacts that depend on track density can cause an

additional 0%–10% loss of reconstructed tracks; so the overall efficiency is typically 85% per event.

The TPC's pseudorapidity coverage of an event is supplemented by two cylindrical and azimuthally symmetric forward time projection chambers (FTPCs). The FTPCs are placed in the forward and backward direction relative to the main TPC and cover pseudorapidity intervals $2.7 < |\eta| < 3.9$ [26]. In the most forward direction, STAR has two zero-degree-calorimeter–shower maximum detectors (ZDC-SMDs) [27,28], which are sensitive to the directed flow of neutrons in the beam rapidity regions.

A minimum bias trigger was used during data taking. Events with a primary vertex within 30 cm along the beam line from the center of the main TPC were selected for the analysis. Standard STAR software cuts were applied to suppress pileup and other malformed events or tracks. The results presented here are based on 14.7M Au + Au and 13.9M Cu + Cu events at the center-of-mass energy of a nucleon pair $\sqrt{s_{NN}} = 200$ GeV and 2.4M Au + Au and 6.3M Cu + Cu events at $\sqrt{s_{NN}} = 62$ GeV. The data were taken with the magnetic field in the full field (FF) and reverse full field (RFF) configurations with the strength of the magnetic field at 0.5 T. The centrality of the collision is determined according to the reference multiplicity (refMult), which is the recorded multiplicity of charged particles in $|\eta| < 0.5$ that satisfy specific track quality cuts.

The correlations are reported in the pseudorapidity region $|\eta| < 1.0$ covered by the main TPC. For this analysis, the tracks in the TPC are required to have $p_t > 0.15$ GeV/c. For the results integrated over transverse momentum we also impose an upper cut of $p_t < 2$ GeV/c. Standard STAR track quality cuts are applied: A minimum of 15 tracking points are required for a track to be considered good. The ratio of the number of hit points on a track to the maximum possible given the track geometry is required to be greater than 0.52 to avoid the effects of track splitting. The data with reverse magnetic field were used to assess systematic effects as the biases for positive and negative charged particles interchange. The final results reported here are averaged over both field polarities.

We use particle identification via specific energy loss (dE/dx) in the volume of the TPC to reject electrons as a check that the signal we present is determined by hadron production.

III. METHOD

In practice, the reaction plane angle for a given collision is not known. To evaluate the correlator defined in Eq. (4), one estimates the reaction plane with the so-called event plane reconstructed from particle azimuthal distributions [29]. For the event plane determination one can use particles found in the same detector that is used to detect particles α and β (in our case STAR's main TPC) or different detectors (we have used the STAR FTPCs and the ZDC-SMD). The second-order event plane (determined by the second harmonic modulation in particle distribution) is sufficient for this study. We make use of the large elliptic flow measured at RHIC [30] to determine the event plane from particle distributions in the main and forward TPCs. When using the ZDC-SMD for event-plane reconstruction, the first-order event plane can be determined through the measured directed flow of spectator neutrons.

In the three-particle correlation technique, the explicit determination of the event plane is not required; instead, the role of the event plane is played by the third particle that enters the correlator with double the azimuth [21,23,29]. Under the assumption that particle c is correlated with particles α and β only via common correlation to the reaction plane, we have

$$\langle\cos(\phi_a + \phi_\beta - 2\phi_c)\rangle = \langle\cos(\phi_a + \phi_\beta - 2\Psi_{\mathrm{RP}})\rangle\, v_{2,c}, \qquad (7)$$

where $v_{2,c}$ is the elliptic flow value of the particle c. We check this assumption by using particles c from different detectors and exhibiting different elliptic flow. We also study the effect of using only positive or only negative particles to determine the event plane and compare the results obtained with different field polarities in our estimates of the systematic uncertainties. All the correlators presented in this article have been calculated by first averaging over all particles under study in a given event and subsequently averaging the results over all events in a given event sample.

The STAR TPCs have quite uniform azimuthal acceptance. Nevertheless, TPC sector boundaries, malfunctioning electronics, etc., may introduce biases in the analysis, in particular as the acceptance for positive and negative particles is different. To avoid these effects, we use a recentering procedure [29] in which we substitute $\cos\phi \to \cos\phi - \langle\cos\phi\rangle$ and $\sin\phi \to \sin\phi - \langle\sin\phi\rangle$ and similarly for the second harmonic. The typical values of $\langle\cos\phi\rangle$ and $\langle\sin\phi\rangle$ for the tracks in the main TPC are $\lesssim$0.003, but for high-p_t particles and the most central collisions could go as high as 0.015. In the FTPC region, the typical correction is of the order of a few percent. The validity of the recentering method can be verified by calculating three-particle cumulants [20,31]:

$$\begin{aligned}&\langle\cos(\phi_\alpha + \phi_\beta - 2\phi_c)\rangle \\ &\quad = \Re\left\{\left\langle\left\langle u_\alpha u_\beta v_c^2\right\rangle\right\rangle + \langle u_\alpha u_\beta\rangle\left\langle v_c^2\right\rangle + \left\langle u_\alpha v_c^2\right\rangle\langle u_\beta\rangle \right. \\ &\qquad \left. + \left\langle u_\beta v_c^2\right\rangle\langle u_\alpha\rangle - 2\langle u_\alpha\rangle\langle u_\beta\rangle\left\langle v_c^2\right\rangle\right\}, \end{aligned} \qquad (8)$$

where we use notations $u = e^{i\phi}$ and $v = u^* = e^{-i\phi}$. $\Re\{\ldots\}$ denotes the real part, and double angle brackets denote cumulants. In the case of perfect acceptance, the cumulant $\langle\langle\cos(\phi_\alpha + \phi_\beta - 2\phi_c)\rangle\rangle$ coincides with the correlator $\langle\cos(\phi_\alpha + \phi_\beta - 2\phi_c)\rangle$. As can be seen from Eq. (8), to account for the acceptance effect, it is sufficient to perform a recentering procedure. All results presented in this article have been corrected for acceptance effects, where applicable, by this method. The cumulant Eq. (8) can be calculated directly by correcting the three-particle correlator with the corresponding products of two- and single-particle averages. We have compared the results obtained by directly calculating cumulants with the results obtained by the recentering method and found them to be consistent. Because the detector acceptance varied during the period of data taking, we perform the corresponding correction run by run, separately for positive and negative particles, and for each centrality bin. We also account for the acceptance dependence on particle pseudorapidity and transverse momentum. We consider separately the east ($\eta < 0$) and west ($\eta > 0$) FTPCs. We have found that the corrections

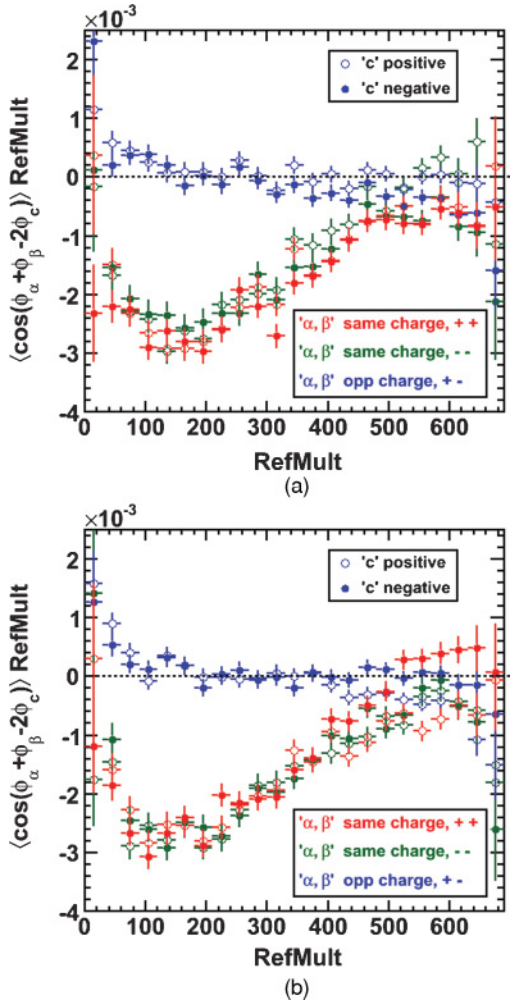

FIG. 3. (Color) $\langle\cos(\phi_\alpha + \phi_\beta - 2\phi_c)\rangle$ as a function of reference multiplicity for different charge combinations, before corrections for acceptance effects. In the insets the signs indicate the charge of particles α, β, and c. The results shown are for Au + Au collisions at 200 GeV obtained in (a) the reversed full field, and (b) the full field configurations.

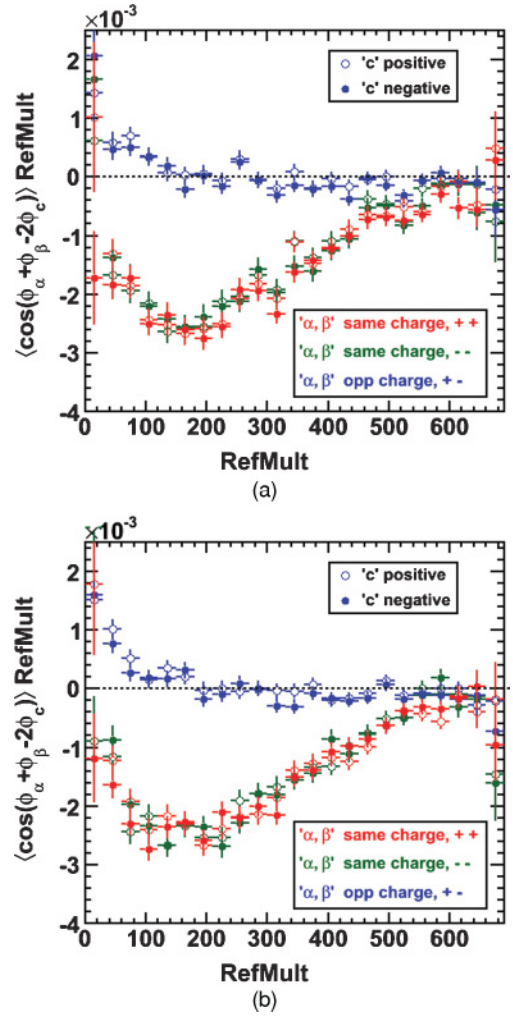

FIG. 4. (Color) Same as Fig. 3 after correction for acceptance effects.

do not depend significantly on the collision vertex position along the beam line.

IV. DETECTOR EFFECT STUDIES

Figure 3 shows the three-particle correlator [Eq. (7)] as a function of reference multiplicity in Au + Au collisions at $\sqrt{s_{NN}} = 200$ GeV for two field polarities before the recentering procedure. All three particles are from the main TPC region, $|\eta| < 1.0$. Figure 4 shows results for the same correlator after correction. The correlator has been scaled by the reference multiplicity for clarity at high centralities, where the absolute values of the signal are small. These figures are intended only to illustrate the effect of the recentering; for that reason and also to have finer binning in centrality, we plot the correlator directly versus reference multiplicity. All other results are presented as a function of the fraction of the total interaction cross section (which is calculated taking into account the track, event vertex reconstruction, and trigger inefficiencies). The acceptance effects are most noticeable for central collisions, where the signal is small; there is a slight difference in results depending on whether the third (c) particle is positive or negative and the difference changes sign depending on the polarity of the magnetic field. This difference disappears after the acceptance correction. Results for particles α and β being both positive or both negative are consistent within statistical errors, and later we combine them as same-charge correlations. As expected for the case when particles α and β are correlated to the particle c only via common correlation to the reaction plane, the results do not depend on the charge of the particle c.

The acceptance effects are larger in the average correlation, $\langle\cos(\phi_\alpha - \phi_\beta)\rangle$, than in the correlator $\langle\cos(\phi_\alpha + \phi_\beta - 2\Psi_{\mathrm{RP}})\rangle$, because the latter represents the difference in correlations projected onto the reaction plane and to the direction normal to the reaction plane. Because the reaction plane is uniformly distributed in azimuth, many of the possible acceptance effects average out to zero.

Figure 5 presents the correlator $\langle\cos(\phi_\alpha - \phi_\beta)\rangle$ for different charge combinations from the Au + Au 200-GeV data

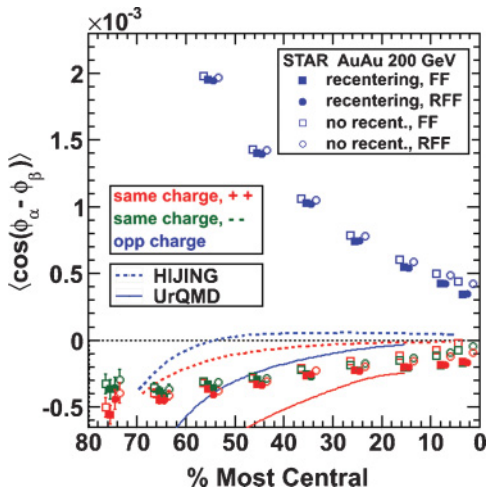

FIG. 5. (Color) $\langle\cos(\phi_\alpha - \phi_\beta)\rangle$ as a function of centrality for different charge combinations and FF and RFF configurations. The data points corresponding to different charge and field configurations are slightly shifted in the horizontal direction with respect to each other for clarity. The error bars are statistical. Also shown are model predictions described in Sec. VII.

obtained with FF and RFF magnetic field settings as a function of collision centrality. In this figure and later in the article, the centrality is quantified by the fraction of the total interaction cross section, with the centrality bins corresponding to (ordered from most to least central) 0%–5%, 5%–10%, 10%–20%, . . . ,70%–80% of the most central collisions. The points are plotted at the middle of the bin, not reflecting possible small biases due to higher weight of events with larger multiplicity within the bin. Before acceptance corrections are applied, $(+, +)$ correlations are slightly different from $(-, -)$ correlations, with the difference changing sign in different field orientations. After the correction, the results from different field polarities coincide with each other.

We have performed several additional checks to ensure that the signal is not attributable to detector effects. High accelerator luminosity leads to significant charge buildup in the TPC, which leads to distortions in the recorded track positions, affecting the reconstructed momenta. We have compared the results obtained from the 2002 RHIC run (a low-luminosity run), with results from 2004–2005 divided into high- and low-luminosity events (selection is based on a ZDC coincidence rate). All three data samples yield the same signal within statistical uncertainties.

The acceptance of the detector depends weakly on the position of the event vertex relative to the center of the TPC. We applied the acceptance corrections differentially according to the event vertex position and explicitly checked the dependence of the signal on the vertex position. No dependence has been found.

The main TPC consists of two parts, which are separated by a central membrane. A particle track will occasionally cross the central membrane and be separately reconstructed in each half-barrel of the TPC. These two track parts can be displaced, one with respect to the other. To check that this effect does not contribute to the signal, we calculated the correlator using only tracks that do not cross the membrane. Taking into account the signal dependence on the track separation in pseudorapidity, the observed signal was found to be consistent with the signal obtained without such a requirement.

Tracks in the TPC are characterized by the distance of closest approach (DCA), the distance between the projection of the track and the event vertex. Particles originating from weak decays (Λ, K_s, etc.) can have larger DCAs than the direct primary particles we are studying. We compared the results obtained with a cut DCA < 1 cm to those of DCA < 3 cm and found only negligible differences with a somewhat larger signal (of the order of the statistical error) for tracks with DCA < 1 cm.

The correlator used in this analysis is the difference between the correlations projected onto the reaction plane and the correlations projected onto the direction normal to the reaction plane. The correlator calculated by projecting onto an axis rotated by $\pi/4$ relative to the reaction plane should only be nonzero owing to detector effects. We have explicitly calculated the correlator in this rotated frame and found it to be zero within statistical error.

Figure 6(a) compares the three-particle correlations obtained for different charge combinations, as a function of centrality, when the third particle is selected from the main TPC with when it is selected from the forward TPCs. Assuming that the second harmonic of the third particle is correlated with the first harmonic of the first two particles via a common correlation to the reaction plane, the correlator should then be proportional to the elliptic flow of the third particle. On average, the elliptic flow in the FTPC region is significantly smaller than that in the TPC region [32], explaining the different magnitudes of the three-particle correlations shown in Fig. 6(a).

Figure 6(b) shows the three-particle correlator after it has been divided by v_2 of the third particle, according to Eq. (7). Resulting signals are in very good agreement in the two cases. In this and subsequent plots, for the elliptic flow of particle c in the main TPC region we use estimates obtained from the correlations of particles in the main TPC region, $|\eta| < 1.0$, with particles in the FTPC, $2.7 < |\eta| < 3.9$. These estimates are less affected by nonflow effects, compared to elliptic flow derived from two-particle correlations with both particles taken from the main TPC.

The shaded band in Fig. 6(b) and the subsequent figures illustrate the systematic change in the results that occur when different estimates of the elliptic flow are used. The upper (in magnitude) limit is obtained with flow from four-particle correlations and the lower limit from the two-particle cumulant method. All elliptic flow data have been taken from Refs. [32,33].[2] Four-particle cumulant values are not available

[2]In Ref. [32,33] an estimate of elliptic flow in the main TPC region, $|\eta| < 1.0$, obtained from correlations of particles in this region with those in FTPCs was denoted as $v_2\{\text{FTPC}\}$; an estimate from two-particle correlations with both particles in the main TPC as $v_2\{2\}$. Elliptic flow from four-particle correlations, denoted as $v_2\{4\}$, is considered to be least affected by nonflow effects. For a review of flow measurements, see Ref. [18].

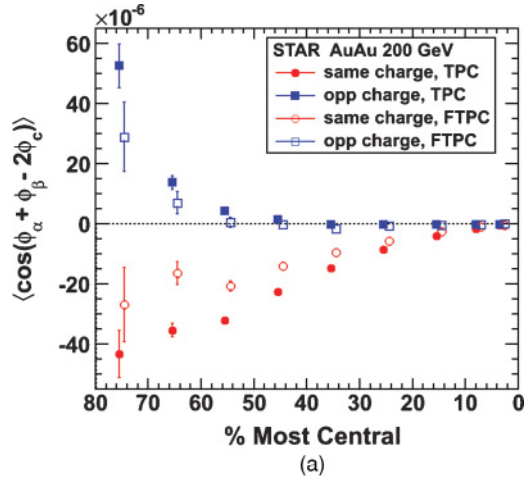

FIG. 6. (Color online) (a) A comparison of the correlations obtained by selecting the third particle from the main TPC or from the forward TPCs. (b) The results after scaling by the flow of the third particle. The shaded areas represent the uncertainty from $v_{2,c}$ scaling (see text for details). In both panels, the TPC and FTPC points are shifted horizontally relative to one another for clarity purposes. The error bars are statistical.

for all collision systems and energies studied here. Therefore, in Figs. 7–9, we plot systematic upper limits obtained with extrapolation of available data assuming that the measurements with FTPC suppress only 50% of the nonflow contribution. The magnitude of the elliptic flow in the FTPC region was estimated from correlations between particles in the east and west FTPCs. Section V has further details on the systematic uncertainties associated with different v_2 estimates.

Results obtained with the event plane reconstructed with ZDC-SMD are consistent with those shown in Fig. 6(b), though the statistical errors on ZDC-SMD results are about 5 times larger because the (second-order) reaction plane resolution from ZDC-SMD is worse.

Figure 6(b) shows very good agreement between the same-charge correlations obtained with the third particle in the TPC and FTPC regions, which supports for such correlations the assumption $\langle\cos(\phi_\alpha + \phi_\beta - 2\Psi_{\rm RP})\rangle \approx \langle\cos(\phi_\alpha + \phi_\beta - 2\phi_c)\rangle / v_{2,c}$. The opposite-charge correlations are small

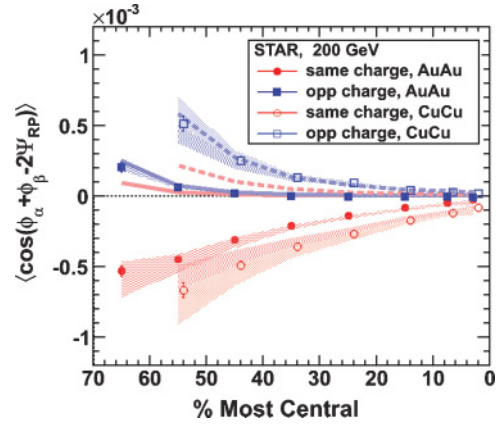

FIG. 7. (Color online) $\langle\cos(\phi_a + \phi_\beta - 2\Psi_{\rm RP})\rangle$ in Au + Au and Cu + Cu collisions at $\sqrt{s_{NN}} = 200$ GeV calculated using Eq. (7). The error bars show the statistical errors. The shaded areas reflect the uncertainty in the elliptic flow values used in calculations, with lower (in magnitude) limit obtained with elliptic flow from two-particle correlations and upper limit from four-particle cumulants. For details, see Sec. IV. Thick solid (Au + Au) and dashed (Cu + Cu) lines represent possible non-reaction-plane-dependent contribution from many-particle clusters as estimated by HIJING (see Sec. VII A).

in magnitude and it is difficult to conclude on validity of the assumption for such correlations based only on results presented in Fig. 6(b). Similarly, in the most peripheral collisions, the statistical errors are large, which also prohibits making a definite conclusion.

V. SYSTEMATIC UNCERTAINTIES

There is one class of uncertainties, related to the question of factorization of Eq. (7), which would arise if the events contained a large number of correlated groups of particles such as minijets. Even if these "clusters" were produced

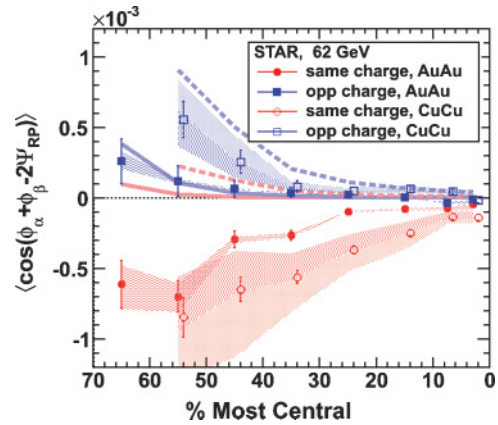

FIG. 8. (Color online) $\langle\cos(\phi_a + \phi_\beta - 2\Psi_{\rm RP})\rangle$ in Au + Au and Cu + Cu collisions at $\sqrt{s_{NN}} = 62$ GeV calculated using Eq. (7). The error bars indicate the statistical errors. The shaded areas reflect the uncertainty in the elliptic flow values used in calculations. For details, see Sec. IV. Thick solid (Au + Au) and dashed (Cu + Cu) lines represent possible non-reaction-plane-dependent contribution from many-particle clusters as estimated by HIJING (see Sec. VII A).

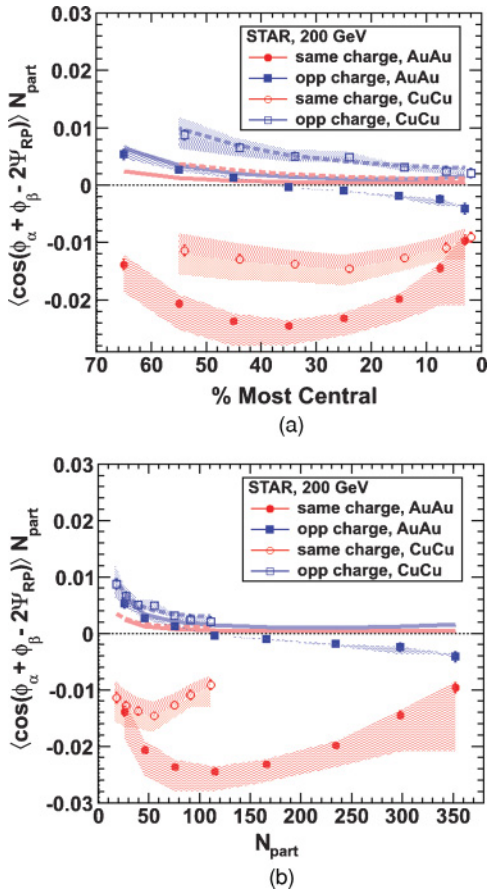

FIG. 9. (Color online) Au + Au and Cu + Cu collisions at $\sqrt{s_{NN}} = 200$ GeV. The correlations are scaled with the number of participants and are plotted as function of (a) centrality and (b) number of participants. The error bars indicate the statistical errors. The shaded areas reflect the uncertainty in the elliptic flow values used in calculations. For details, see Sec. IV. Thick solid (Au + Au) and dashed (Cu + Cu) lines represent possible non-reaction-plane-dependent contribution from many-particle clusters as estimated by HIJING (see Sec. VII A).

isotropically in azimuth, they might contribute to our observable through correlations between the particles used to determine the reaction plane [particle c in Eq. (7)] and the particles (α,β) used to measure the signal. We consider this effect in detail in Sec. VII. As will be shown there, in Cu + Cu and peripheral Au + Au collisions this effect could cause opposite-charge correlations of the sign and magnitude we observe but does not produce the same-charge correlations.

We proceed with discussion of the results assuming $\langle\cos(\phi_\alpha + \phi_\beta - 2\Psi_{\rm RP})\rangle = \langle\cos(\phi_\alpha + \phi_\beta - 2\phi_c)\rangle / v_{2,c}$ but indicate in all plots the HIJING [34] (default, quenching-off settings) three-particle correlation results. The latter can be considered as an estimate of the systematic uncertainty from correlations not related to the reaction plane. In future high-statistic measurements, such uncertainty can be decreased by taking particle c from a rapidity region separated from particles α and β.

One dominant systematic uncertainty in the correlator $\langle\cos(\phi_\alpha + \phi_\beta - 2\Psi_{\rm RP})\rangle$ is attributable to uncertainty in the elliptic flow measurements of the particle used to determine the reaction plane. This contributes a fractional uncertainty, on average of the order of 15% and somewhat larger in most peripheral and most central collisions [32].

From comparison of the results obtained in different field configurations and other studies presented in Sec. IV we conclude that after acceptance corrections are performed, the remaining systematic uncertainties in three-particle correlations owing to detector effects are comparable to or smaller than the statistical errors.

We have performed an additional study to estimate the size of possible error caused by acceptance effects before and after the recentering correction is applied: We have run simulations in which tracks were generated using realistic single-particle distributions but having no correlation except owing to elliptic flow. An efficiency loss is introduced similar to that of the STAR detector as a function of azimuth, transverse momentum, and particle charge. We then study the effect of distorting the efficiency in additional and more extreme ways. In all of these cases, after the recentering correction is applied, the value of $\langle\cos(\phi_\alpha + \phi_\beta - 2\phi_c)\rangle$ is zero for all centralities within the statistical precision of the study, which is about 3×10^{-6} for the most peripheral bin and decreases to less than 10^{-7} for the most central bin. This is many times smaller than the measured signal for all centralities in all cases.

Errors in measuring the magnitude of particle momenta make negligible contributions to the correlator used in this analysis, which uses only measured azimuthal angles. It is therefore robust against many systematic errors which are commonly encountered in the analyses of the STAR data (space charge distortion errors leading to momentum biases, etc.).

Theoretical treatments of the correlator defined in Eq. (4) were developed with charged hadrons in mind. By using cuts (based on specific energy loss) to suppress the presence of electrons in our sample, we have verified that this bias is also smaller than the statistical errors.

VI. RESULTS

Final results presented in this section have been obtained with three-particle correlation using Eq. (7) with all three particles from the pseudorapidity region $|\eta| < 1.0$. Figure 7 presents the correlator $\langle\cos(\phi_\alpha + \phi_\beta - 2\Psi_{\rm RP})\rangle$ for Au + Au and Cu + Cu collisions at $\sqrt{s_{NN}} = 200$ GeV. Positive-positive and negative-negative correlations are found to be the same within statistical errors [see Fig. 4(b)] and are combined together as same-charge correlations. Opposite-charge correlations are relatively smaller than same-charge correlations, in agreement with possible suppression of the back-to-back correlations discussed in the Introduction. The correlations in Cu + Cu collisions, shown as open symbols, appear to be larger than the correlations in Au + Au for the same centrality of the collision. One reason for this difference may be the difference in number of participants (or charge multiplicity) in Au + Au and Cu + Cu collisions at the same centrality. The signal is expected to have a $1/N$ dependence, and at the same

centrality of the collision the multiplicity is smaller in Cu + Cu collisions than in Au + Au. The difference in magnitude between same- and opposite-charge correlations is considerably smaller in Cu + Cu than in Au + Au, qualitatively in agreement with the scenario of stronger suppression of the back-to-back correlations in Au + Au collisions. In Fig. 7 and later in the article, error bars indicate statistical uncertainties. The shaded bands show the systematic uncertainty associated with measurements of elliptic flow which are used to rescale the three-particle correlator. In this section we assume the factorization of correlator Eq. (7). The possible error owing to this assumption—which may be large for peripheral bins in the opposite-charge correlation—is denoted by the thick lines in Fig. 7 and subsequent figures and is explained in Sec. VII. Other systematic uncertainties have been discussed in Sec. V.

Figure 8 shows results for collisions at $\sqrt{s_{NN}} = 62.4$ GeV. The signal is similar in magnitude, with slightly more pronounced opposite-charge correlations compared to those at $\sqrt{s_{NN}} = 200$ GeV. This is consistent with weaker suppression of opposite-charge correlations in the less dense 62-GeV system.

The correlations are weaker in more central collisions compared to more peripheral collisions, which partially can be attributed to dilution of correlations, which occurs in the case of particle production from multiple sources. To compensate for this effect and to present a more complete picture of the centrality dependence, we show in Fig. 9 results multiplied by the number of participants. The number of nucleon participants is estimated from a Monte-Carlo Glauber model [35]. Figure 9(a) presents the results as a function of centrality, and Fig. 9(b) presents the results as a function of $N_{\rm part}$. Smaller correlations in most central collisions are expected in the $\mathcal{P}$-violation picture as the magnetic field weakens. The same- and opposite-charge correlations clearly exhibit very different behavior. Figure 9(a) demonstrates that the same-charge correlations show similar centrality dependencies, as would be expected if the geometry of the collision is important. The opposite-charge correlations in Au + Au and Cu + Cu collisions are found to be close at similar values of $N_{\rm part}$, in rough qualitative agreement with the picture in which their values are mostly determined by the suppression of back-to-back correlations.

Figure 10 shows the dependence of the signal on the difference in pseudorapidities of two particles, $\Delta\eta = |\eta_\alpha - \eta_\beta|$, for 30%–50% and 10%–30% centralities. The signal has a typical hadronic width of about one unit of pseudorapidity. The dependence on $|\eta_\alpha - \eta_\beta|$ has been calculated for all charged tracks with $0.15 < p_t < 2.0$ GeV/c. Figure 11 shows the dependence of the signal on the sum of the transverse momentum (magnitudes) of the two particles for these same centralities. Results presented is this figure have no upper p_t cut. We do not observe the signal concentration in the low-p_t region as naively might be expected for $\mathcal{P}$-violation effects.

Figure 12 shows the dependence of the signal on the difference in the magnitudes of the two-particle transverse momenta. We find that the correlation depends very weakly on $|p_{t,\alpha} - p_{t,\beta}|$. This excludes quantum interference (HBT) or Coulomb effects as possible explanations for the signal. There are no specific theoretical predictions on this dependence for the chiral magnetic effect, though naively one expects that the signal should not extend to large values of $|p_{t,\alpha} - p_{t,\beta}|$.

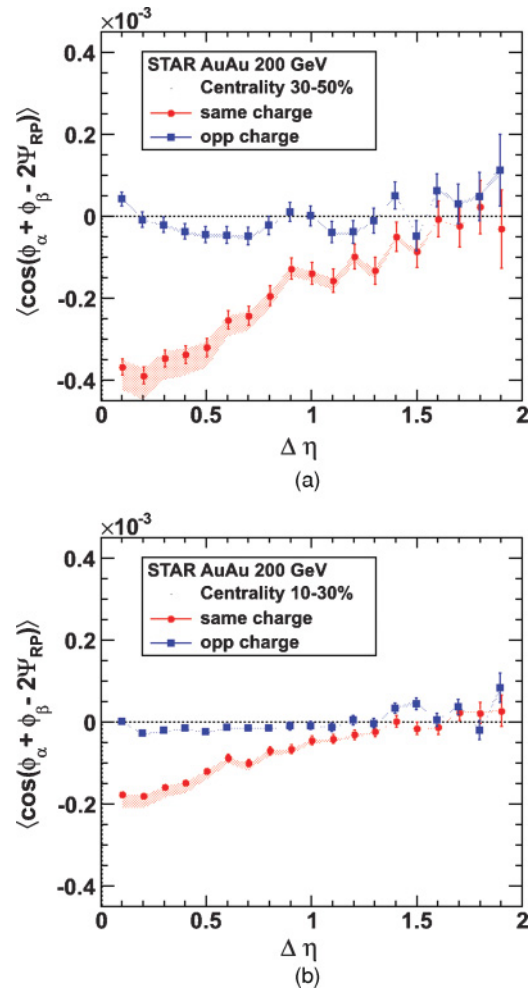

FIG. 10. (Color online) Au + Au at 200 GeV. The correlations dependence on pseudorapidity separation $\Delta\eta = |\eta_\alpha - \eta_\beta|$ for (a) centrality 30%–50% and (b) centrality 10%–30%. The shaded bands indicate uncertainty associated with v_2 measurements and have been calculated using two- and four-particle cumulant results as the limits.

Finally, the ZDC-SMD detector has good first-order reaction-plane resolution. For mid-central collisions, the resolution $\langle\cos(\Psi_1 - \Psi_{\rm RP})\rangle$ is of the order of 0.35–0.4. The ZDC-SMD allows us to test the first-order ($\mathcal{P}$-odd) effect of the charge separation along the system orbital momentum, which would correspond to $\langle a_\alpha\rangle \neq 0$. In theory, this is possible only if the vacuum $\theta \neq 0$. Our measurements are consistent with zero, averaged over all centralities $\langle a_+\rangle = (-0.1 \pm 1.0) \times 10^{-4}$ and $\langle a_-\rangle = (-1.0 \pm 1.0) \times 10^{-4}$.

VII. PHYSICS BACKGROUNDS

A. Reaction-plane-independent background

Reaction-plane-independent background is caused by three (or more) particle clusters which affect the factorization of

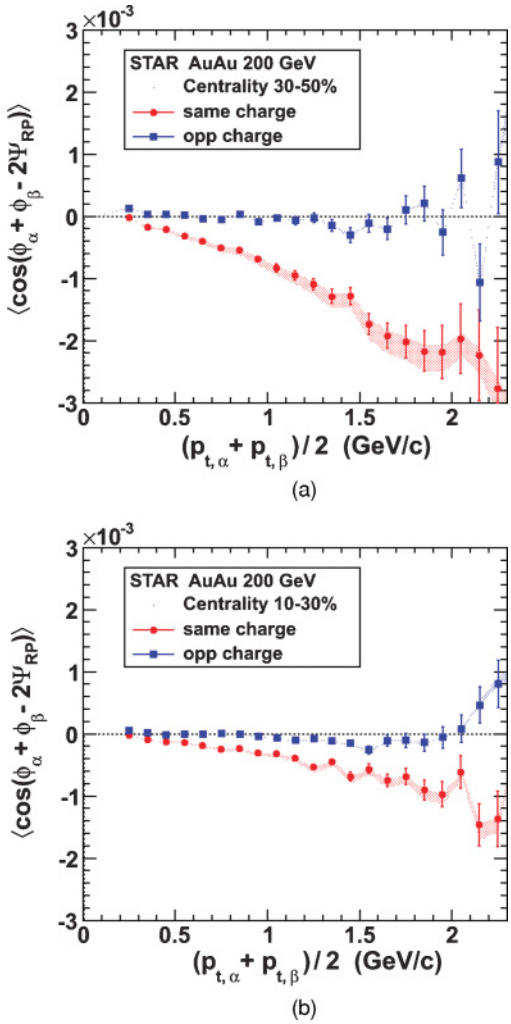

FIG. 11. (Color online) Au + Au at 200 GeV. The correlations dependence on $(p_{t,\alpha} + p_{t,\beta})/2$ for (a) centrality 30%–50% and (b) centrality 10%–30%. The shaded bands have the same meaning as in Fig. 10.

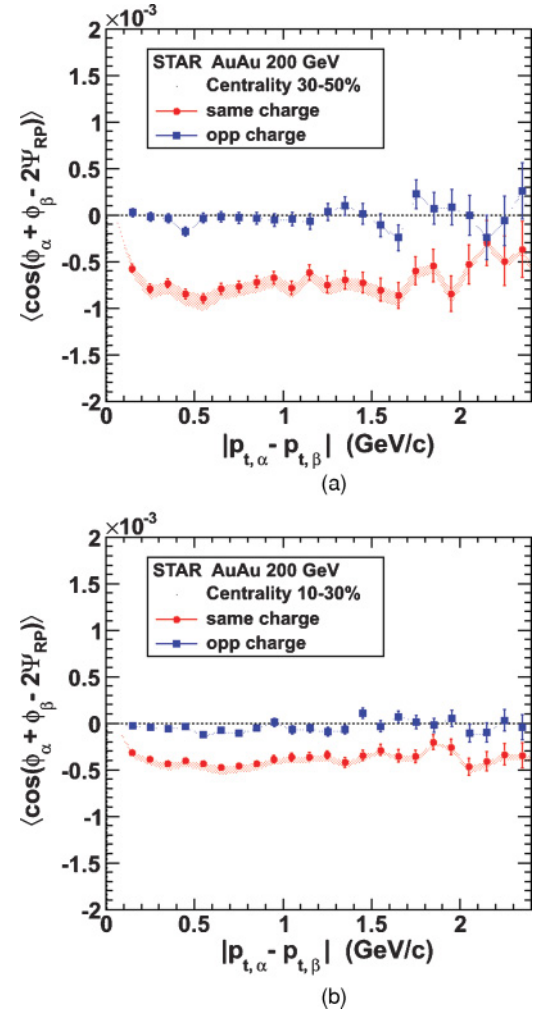

FIG. 12. (Color online) Au + Au at 200 GeV. The correlations dependence on $|p_{t,\alpha} - p_{t,\beta}|$ for (a) centrality 30–50% and (b) centrality 10%–30%. The shaded bands have the same meaning as in Fig. 10.

Eq. (7). With future high-statistics data sets, it will be possible to reduce such backgrounds significantly by determining the reaction plane using particles far remote in rapidity from the signal particles.

To estimate possible contribution to the three-particle correlator of effects not related to the reaction plane orientation, we use the HIJING [34] event generator, which is based on the minijet picture of heavy-ion collisions. For all HIJING results presented in this article we use default, quenching-off setting. Figure 13 presents the results for the three-particle correlator, $\langle\cos(\phi_a + \phi_\beta - 2\phi_c)\rangle$, measured in Au + Au and Cu + Cu collisions as a function of centrality together with HIJING results for the correlations among three particles from many-particle clusters. In this figure the most central points correspond to centrality 0%–5% and the most peripheral to 60%–70% for Au + Au collisions and 50%–60% for Cu + Cu collisions. The correlator is scaled with number of participants for clarity at large centralities, where the signal is small in magnitude. The correlations are shown as a function of the number of participants because this gives very similar HIJING results for Au + Au and Cu + Cu collisions, implying a dependence only on the charged-particle rapidity density. We have separately checked that HIJING results scale as N^{-2}, as expected for contributions from many-particle clusters. Figure 13 shows that if this minijet picture in HIJING is correct, in peripheral collisions the entire opposite-charge signal may be dominated by contributions from clusters not related to the reaction-plane orientation. The same-charge correlations in HIJING are significantly smaller in magnitude than in data and have opposite sign. HIJING results for three-particle correlations among three particles all of the same charge are consistent with zero, in sharp contrast to the data shown in Fig. 4.

We have also studied such reaction-plane-independent backgrounds using the event generator URQMD [36] and found that the predicted contributions to both opposite-charge and same-charge correlations are at least a factor of two lower than those predicted by HIJING.

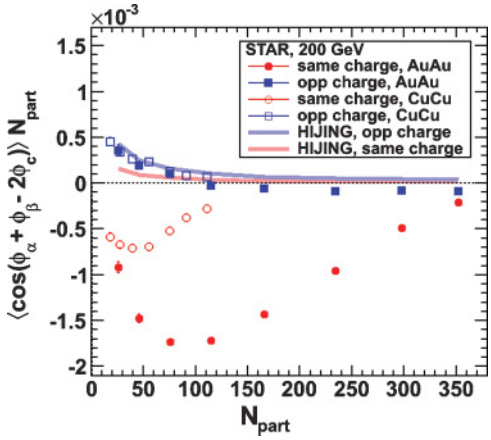

FIG. 13. (Color online) Three-particle correlator in Au + Au and Cu + Cu collisions compared to HIJING calculations shown as thick lines. All three particles are taken in the main TPC region, $|\eta| < 1.0$. The correlator has been scaled with number of participants and is plotted versus number of participants. In this representation HIJING results for Au + Au and Cu + Cu collisions coincide in the region of overlap.

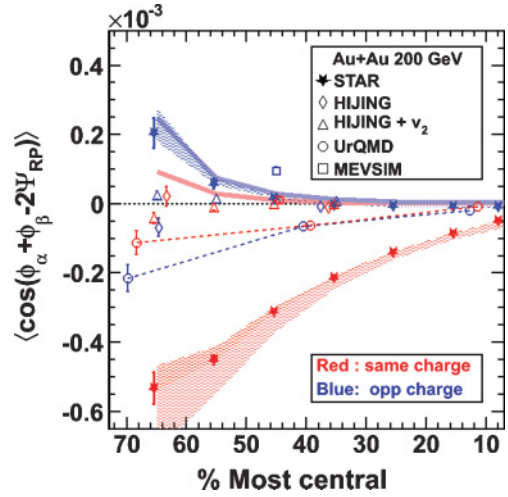

FIG. 14. (Color) $\langle\cos(\phi_\alpha + \phi_\beta - 2\Psi_{\rm RP})\rangle$ calculated for 200-GeV Au + Au events with event generators HIJING (with and without an "elliptic flow afterburner"), URQMD, and MEVSIM. Blue symbols mark opposite-charge correlations, and red are same-charge. Solid stars represent the values from the data to facilitate comparison. Acceptance cuts of $0.15 < p_t < 2$ GeV/c and $|\eta| < 1.0$ were used in all cases. For MEVSIM, HIJING, and URQMD points the true reaction plane from the generated event was used for $\Psi_{\rm RP}$. Thick, solid lighter-colored lines represent possible non-reaction-plane-dependent contribution from many-particle clusters, as estimated by HIJING and discussed in Sec. VII A. Corresponding estimates from URQMD are about factor of two smaller.

B. Reaction-plane-dependent background

Unlike those discussed in Sec. VII A, reaction-plane-dependent physics backgrounds can not be suppressed by better methods of determining the reaction plane.

The correlator $\langle\cos(\phi_\alpha + \phi_\beta - 2\Psi_{\rm RP})\rangle$ is a $\mathcal{P}$-even observable and can exhibit a nonzero signal for effects not related to $\mathcal{P}$ violation. Among those are processes in which particles α and β are products of a cluster (e.g., resonance, jet, dijets) decay, and the cluster itself exhibits elliptic flow [21,23] or decays (fragments) differently when emitted in plane compared to out of plane.

If "flowing clusters" are the only contribution to the correlator, we can write

$$\begin{aligned}&\langle\cos(\phi_\alpha + \phi_\beta - 2\Psi_{\rm RP})\rangle\\ &\quad = A_{\rm clust}\,\langle\cos((\phi_\alpha + \phi_\beta - 2\phi_{\rm clust}) + 2(\phi_{\rm clust} - \Psi_{\rm RP}))\rangle_{\rm clust}\\ &\quad = A_{\rm clust}\,\langle\cos(\phi_\alpha + \phi_\beta - 2\phi_{\rm clust})\rangle_{\rm clust}\, v_{2,\rm clust},\end{aligned} \tag{9}$$

where $\langle\cdots\rangle_{\rm clust}$ indicates that the average is performed only over pairs consisting of two daughters from the same cluster and the resulting normalization factor is $A_{\rm clust} = N_{\frac{\rm clust}{\rm event}} N_{\frac{\rm pairs}{\rm clust}} / N_{\frac{\rm pairs}{\rm event}}$. Equation (9) assumes that there is no reaction-plane dependence of $\cos(\phi_\alpha + \phi_\beta - 2\phi_{\rm clust})$. The term $\langle\cos(\phi_\alpha + \phi_\beta - 2\phi_{\rm clust})\rangle$ is a measure of the azimuthal correlations of decay products with respect to the cluster azimuth, while $v_{2,\rm clust}$ is cluster elliptic flow. In the case of resonance decays, $\langle\cos(\phi_\alpha + \phi_\beta - 2\phi_{\rm res})\rangle$ is zero if the resonance is at rest and becomes nonzero only owing to resonance motion. Estimates of the contribution of "flowing resonances," based on Eq. (9) and reasonable values of resonance abundances and values of elliptic flow, indicate that they should not produce a fake signal. Given the relative scarcity of parents decaying to two same-charge daughters, a much smaller magnitude is expected for same-charge than opposite-charge correlations from this source. Kinematic studies demonstrate that it is very difficult for the sign of the correlations observed in the data to be created in the same-charge correlations without postulating a negative value of v_2 for the resonances or particles from cluster decays.

To study the contribution from resonances in greater detail, we have carried out simulations using the MEVSIM event generator [37]. MEVSIM generates particles according to the single-particle momentum distributions measured at RHIC. The only correlations included are an overall bulk elliptic flow pattern and correlations between daughters of the same resonance decay (resonances included are ϕ, Δ, ρ, ω, and K^*). MEVSIM simulation results are shown as solid squares in Fig. 14; the opposite-charge correlations are larger than what is seen in the data, while the same-charge correlations are far smaller in magnitude and of the wrong sign to match $\mathcal{P}$-violation correlations. We conclude that resonances are not responsible for the observed signal.

In addition to contributing to reaction-plane-independent background, as discussed in Sec. VII A, jets are another potential source of reaction-plane-dependent background because their properties may vary with respect to the reaction plane. For those jets in a heavy-ion event that include a charged particle of sufficiently high p_t to act as a trigger particle for a jet analysis, we may estimate the contribution using the results of previous STAR jet studies [38–40]. With trigger transverse momentum values that allow such analysis ($p_t > 3$ GeV/c) the contribution to $\langle\cos(\phi_\alpha + \phi_\beta - 2\Psi_{\rm RP})\rangle$ is roughly two orders of magnitude below the same-charge signal shown in Fig. 7.

To extend the study of jet contributions to lower momentum, we rely on event generator (in particular, HIJING) calculations.

Several correlation measurements from RHIC [41,42] and earlier measurements at ISR (see review [22]) indicate that cluster formation plays an important role in multiparticle production at high energies. These clusters, with a size inferred in Ref. [41] to be 2.5–3 charged particles per cluster, may account for production of a significant fraction of all particles. Because we have limited information about the nature of these clusters, we do not make an estimate of their contribution to the observed correlations. Our studies indicate that to fake the same-charge correlations observed in the data, there should be several types of clusters, with some of them having negative values of elliptic flow. It is hoped that with a better understanding of the cause and properties (including charge dependence and v_2) of such clusters, a clearer statement can be made regarding their contributions.

We have also run simulations with several $p+p$ and Au + Au event generators. With PYTHIA [43] $p+p$ events we find that the correlations in $\langle\cos(\phi_\alpha-\phi_\beta)\rangle$ are significantly smaller than those seen in Au + Au data when scaled by $1/N$ and are similar for all charge combinations. We add modulation with respect to the reaction plane by adding v_2 through angular correlations or strong (elliptically modulated) radial flow. This way we create nonzero values for $\langle\cos(\phi_\alpha+\phi_\beta-2\Psi_{\rm RP})\rangle$, albeit with correlations different from the data, being always positive and similar in magnitude for all charge combinations.

Figure 14 shows results for (reaction-plane-dependent) physics backgrounds to $\langle\cos(\phi_\alpha+\phi_\beta-2\Psi_{\rm RP})\rangle$ calculated with 200-GeV Au + Au events from the event generators URQMD [36] and HIJING [34]. Because the modulation of $dN/d\phi$ with respect to the reaction plane is smaller in HIJING than seen in RHIC data, we also run HIJING with an added "afterburner," which adds elliptic flow using as input v_2 values consistent with STAR measurements at the given centrality. Elliptic flow is introduced by the "shifting" method [29], which preserves other correlations that exist in the model. Figure 14 shows that no generator gives qualitative agreement with the data; the model values of $\langle\cos(\phi_\alpha+\phi_\beta-2\Psi_{\rm RP})\rangle$ are significantly smaller in magnitude than what is seen in the data, and the correlations calculated in these models tend to be very similar for same- and opposite-charge correlations.

These models do not match the correlations for $\langle\cos(\phi_\alpha-\phi_\beta)\rangle$ that are seen in the data either, as shown in Fig. 5. HIJING predicts very similar same- and opposite-charge correlations that are much smaller in magnitude than seen in the data. URQMD overestimates the same charge correlations. It predicts opposite-charge correlations that are much smaller in magnitude and opposite in sign from the data. This points to the need for better modeling of two-particle correlations to give quantitatively meaningful comparisons for $\langle\cos(\phi_\alpha+\phi_\beta-2\Psi_{\rm RP})\rangle$.

In Fig. 14 we connect URQMD points by dashed lines to illustrate that the "reference line" for strong $\mathcal{P}$correlations might be not at zero. In this particular case of URQMD, both same- and opposite-charge correlations have values below zero. Note that the same-charge correlations sit somewhat above the opposite-charge correlations, opposite to the expectation from local $\mathcal{P}$ violation.

Directed flow, which on average is zero in a symmetric pseudorapidity interval, can contribute to the correlator $\langle\cos(\phi_\alpha+\phi_\beta-2\Psi_{\rm RP})\rangle$ via flow fluctuations. This effect is of the opposite sign [see Eq. (5)] and is similar for different charge combinations unlike the signal. If one assumes that the amplitude of the fluctuations is of the same order of magnitude as the maximum directed flow in the pseudorapidity interval under study, then the flow fluctuation contribution is no more than 10^{-5} for centrality 30%–60%, significantly smaller than the observed signal.

Global polarization of hyperons [44,45], the phenomenon of the polarization of secondary produced particles along the direction of the system's angular momentum, may also contribute to the correlator [Eq. (4)] via $\mathcal{P}$-odd weak decays. This effect could lead to a charge asymmetry with respect to the reaction plane, which is always pointing in the same direction relative to the orientation of the angular momentum. Our main analysis based on the reaction plane reconstructed from the elliptic flow does not distinguish the direction of the angular momentum, and is susceptible to this effect. However, as we pointed out in Sec. VI, our measurement of charge separation along the system orbital angular momentum is zero based on the first-order reaction plane reconstructed in the ZDC-SMD. Global polarization has also been found to be consistent with zero, $P_{\Lambda,\bar{\Lambda}} < 0.02$ [46].

VIII. SUMMARY

An analysis using three-particle correlations that are directly sensitive to the $\mathcal{P}$-violation effects in heavy-ion collisions has been presented for Au + Au and Cu + Cu collisions at $\sqrt{s_{NN}} = 200$ and 62 GeV. The results are reported for different particle charge combinations as a function of collision centrality, particle separation in pseudorapidity, and particle transverse momentum. Qualitatively, the results agree with the magnitude and gross features of the theoretical predictions for local $\mathcal{P}$ violation in heavy-ion collisions, except that the signal persists to higher transverse momenta than expected [15]. The particular observable used in our analysis is $\mathcal{P}$-even and might be sensitive to non-$\mathcal{P}$-violating effects. So far, with the systematics checks discussed in this article, we have not identified effects that would explain the observed same-charge correlations. The observed signal cannot be described by the background models that we have studied (HIJING, HIJING + v_2, URQMD, MEVSIM), which span a broad range of hadronic physics.

A number of future experiments and analyses are naturally suggested by these results. One of them is the study of the correlation dependence on the energy of the colliding ions. The charge separation effect is expected to depend strongly on the formation of a quark-gluon plasma [15], and the signal might be greatly suppressed or completely absent at an energy below that at which a quark-gluon plasma can be formed.

Improved theoretical calculations of the expected signal and potential physics backgrounds in high-energy heavy-ion collisions are essential to understanding whether the observed signal is attributable to local strong $\mathcal{P}$ violation and to further experimental study of this phenomenon.

ACKNOWLEDGMENTS

We thank D. Kharzeev for discussions on the local strong-$\mathcal{P}$-violation phenomenon and its experimental signatures. We thank the RHIC Operations Group and RCF at BNL and the NERSC Center at LBNL and the resources provided by the Open Science Grid consortium for their support. This work was supported in part by the Offices of NP and HEP within the US DOE Office of Science, the US NSF, the Sloan Foundation, and the DFG cluster of excellence "Origin and Structure of the Universe"; CNRS/IN2P3, RA, RPL, and EMN of France; STFC and EPSRC of the United Kingdom; FAPESP of Brazil; the Russian Ministry of Science and Technology; the NNSFC, CAS, MoST, and MoE of China; IRP and GA of the Czech Republic; FOM of the Netherlands; DAE, DST, and CSIR of the Government of India; the Polish State Committee for Scientific Research; and the Korea Science & Engineering Foundation.

[1] C. Amsler *et al.* (Particle Data Group), Phys. Lett. B **667**, 1 (2008).

[2] I. Arsene *et al.* (BRAHMS Collaboration), Nucl. Phys. A **757**, 1 (2005); B. B. Back *et al.* (PHOBOS Collaboration), *ibid.* **757**, 28 (2005); J. Adams *et al.* (STAR Collaboration), *ibid.* **757**, 102 (2005); K. Adcox *et al.* (PHENIX Collaboration), *ibid.* **757**, 184 (2005).

[3] M. Pospelov and A. Ritz, Phys. Rev. Lett. **83**, 2526 (1999).

[4] C. A. Baker *et al.*, Phys. Rev. Lett. **97**, 131801 (2006).

[5] T. D. Lee, Phys. Rev. D **8**, 1226 (1973).

[6] T. D. Lee and G. C. Wick, Phys. Rev. D **9**, 2291 (1974).

[7] P. D. Morley and I. A. Schmidt, Z. Phys. C **26**, 627 (1985).

[8] D. Kharzeev, R. D. Pisarski, and M. H. G. Tytgat, Phys. Rev. Lett. **81**, 512 (1998); D. Kharzeev and R. D. Pisarski, Phys. Rev. D **61**, 111901(R) (2000).

[9] E. V. Shuryak and T. Schafer, Annu. Rev. Nucl. Part. Sci. **47**, 359 (1997).

[10] D. Diakonov, Prog. Part. Nucl. Phys. **51**, 173 (2003).

[11] S. A. Voloshin, Phys. Rev. C **62**, 044901 (2000).

[12] L. E. Finch, A. Chikanian, R. S. Longacre, J. Sandweiss, and J. H. Thomas, Phys. Rev. C **65**, 014908 (2001).

[13] D. Kharzeev, Phys. Lett. B **633**, 260 (2006).

[14] D. Kharzeev and A. Zhitnitsky, Nucl. Phys. A **797**, 67 (2007).

[15] D. E. Kharzeev, L. D. McLerran, and H. J. Warringa, Nucl. Phys. A **803**, 227 (2008).

[16] K. Fukushima, D. E. Kharzeev, and H. J. Warringa, Phys. Rev. D **78**, 074033 (2008).

[17] S. Voloshin and Y. Zhang, Z. Phys. C **70**, 665 (1996).

[18] S. A. Voloshin, A. M. Poskanzer, and R. Snellings, in Landolt-Boernstein, *Relativistic Heavy Ion Physics,* Vol. 1/23 (Springer-Verlag, 2010), p. 5-54.

[19] S. A. Voloshin, Phys. Rev. C **70**, 057901 (2004).

[20] N. Borghini, P. M. Dinh, and J. Y. Ollitrault, Phys. Rev. C **66**, 014905 (2002).

[21] J. Adams *et al.* (STAR Collaboration), Phys. Rev. Lett. **92**, 062301 (2004).

[22] L. Foa, Phys. Rep. **22**, 1 (1975).

[23] N. Borghini, P. M. Dinh, and J. Y. Ollitrault, Phys. Rev. C **64**, 054901 (2001).

[24] K. H. Ackermann *et al.* (STAR Collaboration), Nucl. Instrum. Methods A **499**, 624 (2003).

[25] M. Anderson *et al.*, Nucl. Instrum. Methods A **499**, 659 (2003).

[26] K. H. Ackermann *et al.*, Nucl. Instrum. Methods A **499**, 713 (2003).

[27] J. Adams *et al.* (STAR Collaboration), Phys. Rev. C **73**, 034903 (2006).

[28] C. Adler, H. Strobele, A. Denisov, E. Garcia, M. Murray, and S. White, Nucl. Instrum. Methods A **461**, 337 (2001); The STAR ZDC-SMD has the same structure as the STAR EEMC SMD: C. E. Allgower *et al.* (STAR Collaboration), *ibid.* **499**, 740 (2003); STAR ZDC-SMD proposal, STAR Note SN-0448 (2003).

[29] A. M. Poskanzer and S. A. Voloshin, Phys. Rev. C **58**, 1671 (1998).

[30] K. H. Ackermann *et al.* (STAR Collaboration), Phys. Rev. Lett. **86**, 402 (2001).

[31] I. Selyuzhenkov and S. Voloshin, Phys. Rev. C **77**, 034904 (2008).

[32] J. Adams *et al.* (STAR Collaboration), Phys. Rev. C **72**, 014904 (2005).

[33] S. A. Voloshin (STAR Collaboration), J. Phys. G **34**, S883 (2007).

[34] M. Gyulassy and X.-N. Wang, Comput. Phys. Commun. **83**, 307 (1994); X. N. Wang and M. Gyulassy, Phys. Rev. D **44**, 3501 (1991).

[35] B. I. Abelev *et al.* (STAR Collaboration), Phys. Rev. C **79**, 064903 (2009).

[36] S. A. Bass *et al.*, Prog. Part. Nucl. Phys. **41**, 255 (1998).

[37] R. L. Ray and R. S. Longacre, arXiv:nucl-ex/0008009.

[38] J. Adams *et al.* (STAR Collaboration), Phys. Rev. Lett. **95**, 152301 (2005).

[39] J. Adams *et al.* (STAR Collaboration), Phys. Rev. Lett. **91**, 172302 (2003).

[40] A. Feng (STAR Collaboration), J. Phys. G **35**, 104082 (2008).

[41] B. Alver *et al.* (PHOBOS Collaboration), Phys. Rev. C **75**, 054913 (2007).

[42] M. Daugherity (STAR Collaboration), J. Phys. G **35**, 104090 (2008).

[43] T. Sjostrand, S. Mrenna, and P. Skands, J. High Energy Phys. 05 (2006) 026.

[44] Z. T. Liang and X. N. Wang, Phys. Rev. Lett. **94**, 102301 (2005).

[45] S. A. Voloshin, arXiv:nucl-th/0410089.

[46] B. I. Abelev *et al.* (STAR Collaboration), Phys. Rev. C **76**, 024915 (2007).